SUPPORTING INFORMATION

Insights into the photoelectrocatalytic lignin oxidation to value-added products using a niobium-doped titanium dioxide photoanode

Daniela F.S. Morais [a,b], Luiza M.G. Sena [a,b], Joana M. Ribeiro [c], Telmo da Silva Lopes [d,b], Paula Dias [d,b], Adélio Mendes [d,b], Carina A.E. Costa [a,b], Alírio E. Rodrigues [a,b], Susana R.S. Pereira [e], Paula C. Pinto [e], Rui A.R. Boaventura [a,b], Carlos J. Tavares [c], Vítor J.P. Vilar [a,b,*], Francisca C. Moreira [a,b,*]

[a] *LSRE-LCM – Laboratory of Separation and Reaction Engineering - Laboratory of Catalysis and Materials, Faculty of Engineering, University of Porto, Rua Dr. Roberto Frias, 4200-465 Porto, Portugal*

[b] *ALiCE – Associate Laboratory in Chemical Engineering, Faculty of Engineering, University of Porto, Rua Dr. Roberto Frias, 4200-465 Porto, Portugal*

[c] *CF-UM-UP – Centre of Physics of Minho and Porto Universities, University of Minho, 4804-533 Guimarães, Portugal*

[d] *LEPABE – Laboratory Process Engineering, Environment, Biotechnology and Energy, Faculty of Engineering, University of Porto, Rua Dr. Roberto Frias, 4200-465 Porto, Portugal*

[e] *RAIZ – Forest and Paper Research Institute, Quinta de São Francisco, 3800-783 Aveiro, Portugal*

[*]Corresponding authors:

Tel.: +351 918257824; E-mail: vilar@fe.up.pt (Vítor J.P. Vilar)

Tel.: +351 914332022; E-mail: franciscam@fe.up.pt (Francisca C. Moreira)

Figure SI-1. Photoanode composed of a TiO_2:Nb photocatalyst coated on a FTO glass substrate measuring 4.0 cm × 4.3 cm. The white strip is the conductive silver paste and is 1 cm wide, resulting in a photocatalyst area of 3.0 cm × 3.3 cm.

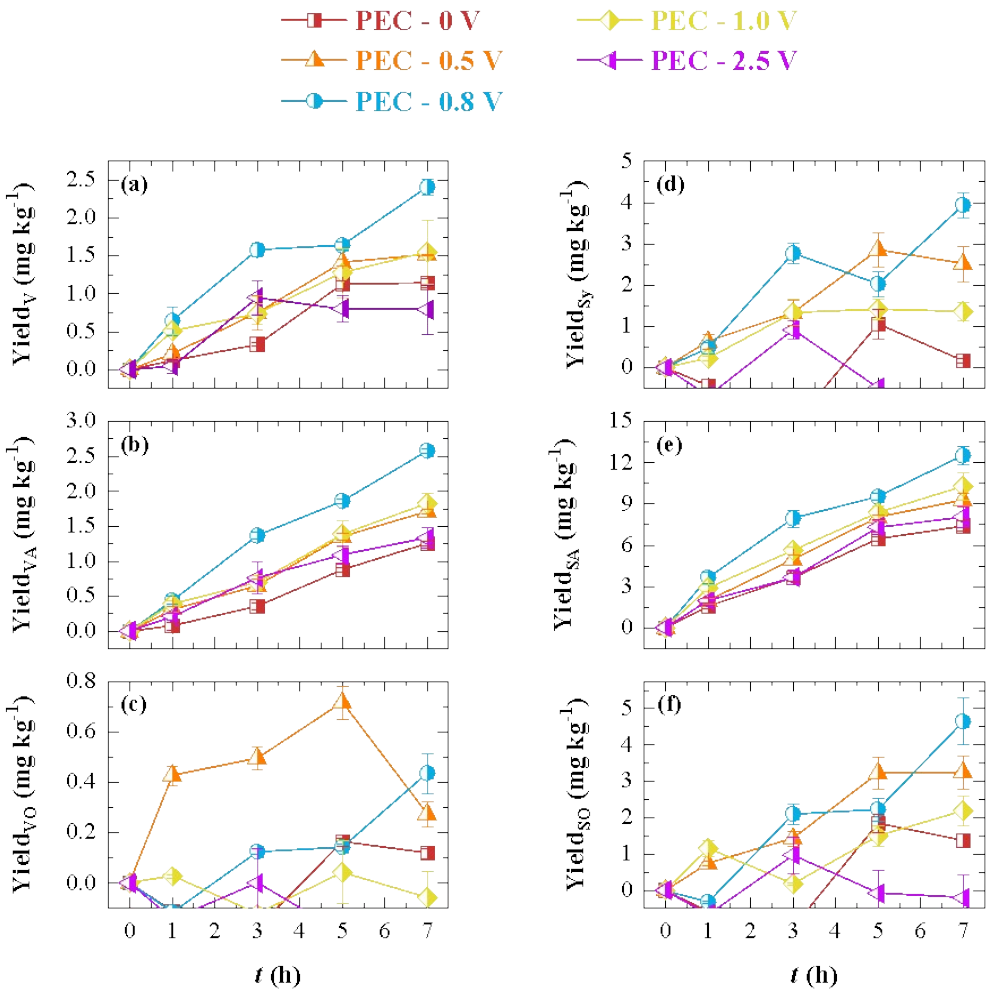

Figure SI-2. Yield to individual LMPPs over time for lignin oxidation using the photoelectrocatalysis (PEC) process at different applied cell potentials: (a) vanillin – V, (b) vanillic acid – VA, (c) acetovanillone – VO, (d) syringaldehyde – Sy, (e) syringic acid – SA, (f) and acetosyringone – SO. Conditions: TiO_2:Nb photoanode; [NaOH] = 1.0 M; $[Lignin]_0$ = 60 g L^{-1}; T = 25±1 ºC; Re = 1750; UVA-LEDs illumination system employed (λ = 365 nm, irradiance = 120±10 mW cm^{-2}) under BSI. All tests were performed in duplicate. Error bars represent error between duplicate trials. *P*-Hydroxybenzaldehyde (pHy) was not detected.

Table SI-1. Reported yields in the literature of LMPPs obtained by nitrobenzene oxidation of lignin isolated from Industrial *Eucalyptus globulus* Kraft liquor.

Lignin type	LMPPs, wt%[a]							Ref.
	pHy	VA	SA	V	Sy	VO	SO	
KL-G	0.3	0.5	3.4	3.4	13.6	NR	NR	[1], [2]
KL-Celbi	NR	NR	NR	1.7	9.5	NR	NR	[2]
WKL	0.1	0.3	2.8	2.6	10.5	NR	NR	[3], [4]
KL-E	0.4	0.4	3.0	2.5	9.4	NR	NR	[1], [2]
KL	NR	NR	NR	2.0	4.4	NR	NR	[5]
KL	0.01	0.2	1.3	1.7	6.9	0.09	0.24	This work

[a] Reported on dry weight and corrected to nonvolatile solids weight after deducing inorganics content; KL-G – lignin isolated from *Eucalyptus globulus* Kraft liquor by a Portuguese mill at the outlet of the Kraft digester; KL-Celbi – lignin isolated from *Eucalyptus globulus* Kraft liquor, supplied by Celbi; WKL – lignin isolated from *Eucalyptus globulus* (weak) Kraft liquor by a Portuguese mill before the evaporation stage; KL-E – lignin isolated from *Eucalyptus globulus* Kraft liquor by a Portuguese mill after the evaporation stage; pHy – *p*-hydroxybenzaldehyde; VA – vanillic acid; SA – syringic acid; V – vanillin; Sy – syringaldehyde; VO – acetovanillone; SO – acetosyringone; NR – not reported.

Table SI-2. FT-IR bands of Kraft liquor lignin and respective assignments.

Experimental band (cm^{-1})		Band assignment		Reference band (cm^{-1})
Raw lignin	Oxidized lignin	Functional group	Attribution	
3385	N/D	O–H	Stretching vibration of phenolic and aliphatic OH	3500-3200 [6]
2939	2939	C–H	Stretching vibration in CH_3	3000-2842 [7] 2960-2925 [8] 2940 [6] 2938-2920 [9] 2937 [10] 2936 [11]
1598	1599	C−C or C=C	Aromatic skeleton stretching vibration	1605-1593 [7] 1600 [8, 12] 1597 [13]
1517	1515	C−C	Aromatic skeleton stretching vibration	1515 [8, 14] 1515-1505 [7] 1514 [11]
1459	1459	C–H	Aromatic skeleton deformation	1470-1455 [9] 1460 [12] 1459 [10]
1424	1421	C−C	Aromatic skeleton stretching vibration	1430-1422 [7] 1426 [13] 1425 [8, 14, 15]
1329	1326	C−O	Stretching of S structure	1335-1320 [9] 1330 [15] 1327 [16] 1326 [8, 12]
1216	N/D	C−O	Ring breathing with C−O stretching of both the S and G structures	*ca.* 1220 [12] 1219 [11] 1216 [15]
1111	1111	C−H	In-plane deformation of S structure	1128-1110 [9] 1115 [8, 12] 1111 [16]
1043	N/D	C–O	Stretching vibration of cellulose, hemicellulose, and lignin	1150-1030 [15] 1041 [13]
N/D	996	C−O	Valence vibration	996-985 [9]
913	913	C–H	Aromatic ring out-of-plane vibration	915 [12]
828	829	C–H	Out-of-plane deformation in G, S and H	832 [10, 13] 831 [11, 12] 825 [8, 16]

N/D – Not detected.

Table SI-3. Quantitative analysis (QA), crystallite size, lattice parameters (*a*, *c*) and preferred orientation derived from the Rietveld fits of the XRD patterns for unused and used TiO_2:Nb thin films.

Sample	Phase	QA (wt%)	Crystallite size (nm)	Unit cell volume (Å³)	*a* (Å)	*c* (Å)	Preferred orientation
TiO_2:Nb unused	TiO_2 rutile	41.1	50	61.5	4.56	2.96	(110), (101)
	TiO_2 anatase	5.4	56	121	3.54	9.66	(101), (103)
TiO_2:Nb used	TiO_2 rutile	64.7	150	61.1	4.54	2.96	N/A
	TiO_2 anatase	N/F	N/F	-	N/F	N/F	N/F

N/A – Not applicable. The sample has low crystallinity, not allowing for well-defined diffraction peaks; N/F – Not found. No evidence of the anatase phase was found on the used TiO_2:Nb thin film.

Table SI-4. O 1s core level XPS fitting parameters.

Sample	Position C1/C2/C3 (eV)	Areas C1/C2/C3 (%)
TiO_2:Nb unused	529.8/530.5/531.9	28/22/50
TiO_2:Nb used	531.6/532.5/533.6	71/29/0

Table SI-5. C 1s core level XPS fitting parameters.

Sample	Position C1/C2/C3 (eV)	Areas C1/C2/C3 (%)
TiO_2:Nb unused	284.9/285.5/288.8	68/26/6
TiO_2:Nb used	284.8/285.4/288.7	56/36/8

Table SI-6. Nb 3d core level XPS fitting parameters.

Sample	Position (eV)	L-S (eV)	Areas $3d_{5/2}/3d_{3/2}$ (%)
TiO_2:Nb unused	206.9	2.8	58/42
TiO_2:Nb used	212.8	N/F	N/F

N/F – Not found.

Table SI-7. Ti 2p core level XPS fitting parameters.

Sample	Position (eV)
TiO_2:Nb unused	458.4
TiO_2:Nb used	462.2

Table SI-8. Consumed charge and electrical consumption (ECo.) for the total reaction time (7 h).

	Charge		ECo.	Yield
	C g_{Lignin}^{-1}	Ah L^{-1}	kWh m^{-3}	mg kg^{-1}
EC – 0.8 V	0.4	0.006	0.004	7
PEC – 0 V	1.2	0.02	-	11
PEC – 0.5 V	2.1	0.03	0.01	19
PEC – 0.8 V	5.0	0.07	0.06	26
PEC – 1.0 V	7.7	0.11	0.10	17
PEC – 2.5 V	24	0.34	0.87	9

2.5. Analytical determinations

2.5.1. HPLC analysis

A VWR-Hitachi LaChrom Elite® liquid chromatograph with a Merck LiChrospher® 100 RP-18 (5 μm) LiChroCART® 125-4 column and a diode array detector (DAD) set at a λ of 280 nm were used. The chromatographic runs were performed at a temperature of 30 ºC and a flow rate of 0.6 mL min^{-1}. A sample volume of 20 μL was injected for each analysis. Since the LMPPs have different polarities, an elution gradient was employed to achieve separation. The mobile phase was composed of MeOH (eluent D) and 10 mM oxalic acid (eluent A). The gradient program was as follows: 0-3 min – 12.5% D, 87.5% A; 7 min – 21.5% D, 78.5% A; 16 min – 32% D, 68% A; 35 min – 51.5% D, 48.5% A; 36-48 min – 12.5% D, 87.5% A. Under these conditions, the seven compounds eluted at the following retention times: pHy at 16.1 min, VA at 16.7 min; SA at 18.3 min; V at 19.0 min; Sy at 20.3 min; VO at 22.0 min; and SO at 22.8 min. To obtain the working calibration curves, standard solutions with all seven LMPPs (pHy, V, Sy, VA, SA, VO, and SO) were prepared by dissolution in MeOH to an individual final concentration of 50 mg L^{-1}. These solutions were further diluted with a 12.5:87.5% (v/v) mixture of MeOH:oxalic acid 10 mM (eluent B) to obtain concentrations between 0.05-25.0 mg L^{-1}. Each standard solution was prepared in duplicate and analyzed in triplicate.

Before HPLC analysis, the resulting LMPPs from lignin oxidation were separated from the KLL solution using solid-phase extraction (SPE) [17]. SPE cartridges (Supelclean™ ENVI™-Chrom P, 80-160 μm, 500 mg, 6 mL) were employed for this procedure. The cartridge was initially equilibrated with 7 mL of eluent D, followed by 14 mL of 87.5:12.5% (v/v) mixture of MeOH:oxalic acid 10 mM (eluent C) and 14 mL of eluent B. The oxidized lignin samples were acidified up to pH 2-3 using a 3 M H_2SO_4 solution, filtered through a 0.20 μm, 25 mm polyethersulfone (PESF) filter, and loaded onto the prepared cartridge using a syringe. The syringe, collection flask, and cartridge were then rinsed with eluent B and thoroughly dried. Finally, the LMPPs were eluted with 7 mL of eluent C and

collected in a 10 mL volumetric flask. The volume was adjusted using the same eluent solution. The extracted LMPPs were subsequently analyzed by HPLC.

2.5.2. pH, temperature, and viscosity

The pH was determined using a Hanna Instruments edge® multiparameter equipped with a HI2020-02 pH electrode. Temperature was determined by a Hanna Instruments HI8424. Viscosity was determined using a glass capillary following ISO 3104:2020 standard test method [18].

Data for this article, including those used to prepare all figures, are available at the following link: https://www.dropbox.com/scl/fi/10ygkb77k9o0hsrwbs5qo/Data.opju?rlkey=d452g8wcq4p8pfx7pzuievcbc&st=uzwc0bso&dl=0

5. References

[1] Pinto, P.C.R., Costa, C.E., Rodrigues, A.E. (2013). Oxidation of lignin from *Eucalyptus globulus* pulping liquors to produce syringaldehyde and vanillin, Industrial & Engineering Chemistry Research 52(12), 4421-4428. https://doi.org/10.1021/ie303349j.

[2] Costa, C.A.E., Vega-Aguilar, C.A., Rodrigues, A.E. (2021). Added-value chemicals from lignin oxidation, Molecules 26(15), 4602. https://doi.org/10.3390/molecules26154602.

[3] Costa, C.A.E., Pinto, P.C.R., Rodrigues, A.E. (2018). Lignin fractionation from E. globulus Kraft liquor by ultrafiltration in a three stage membrane sequence, Separation and Purification Technology 192, 140-151. https://doi.org/10.1016/j.seppur.2017.09.066.

[4] Costa, C.A.E., Casimiro, F.M., Vega-Aguilar, C., Rodrigues, A.E. (2023). Lignin valorization for added-value chemicals: Kraft lignin *versus* lignin fractions, ChemEngineering 7(3), 42. https://doi.org/10.3390/chemengineering7030042.

[5] Villar, J.C., Caperos, A., García-Ochoa, F. (1997). Oxidation of hardwood Kraft-lignin to phenolic derivatives. Nitrobenzene and copper oxide as oxidants, Journal of Wood Chemistry and Technology 17(3), 259-285. https://doi.org/10.1080/02773819708003131.

[6] Yan, P., Xu, Z., Zhang, C., Liu, X., Xu, W., Zhang, Z.C. (2015). Fractionation of lignin from eucalyptus bark using amine-sulfonate functionalized ionic liquids, Green Chemistry 17(11), 4913-4920. https://doi.org/10.1039/c5gc01035g.

[7] Shao, D., Liang, J., Cui, X., Xu, H., Yan, W. (2014). Electrochemical oxidation of lignin by two typical electrodes: Ti/Sb SnO_2 and Ti/PbO_2, Chemical Engineering Journal 244, 288-295. https://doi.org/10.1016/j.cej.2014.01.074.

[8] Tejado, A., Peña, C., Labidi, J., Echeverria, J.M., Mondragon, I. (2007). Physico-chemical characterization of lignins from different sources for use in phenol-formaldehyde resin synthesis, Bioresource Technology 98(8), 1655-1663. https://doi.org/10.1016/j.biortech.2006.05.042.

[9] Popescu, C.-M., Popescu, M.-C., Singurel, G., Vasile, C., Argyropoulos, D.S., Willfor, S. (2016). Spectral characterization of eucalyptus wood, Applied Spectroscopy 61(11), 1168-1177. https://doi.org/10.1366/000370207782597076.

[10] Xiao, X., Sun, S., Qi, Y., Hao, S., Zhang, W., Qiu, X. (2023). Selective electrocatalytic oxidation of C(OH)–C bond in lignin with Pt@CeO_2 toward the synthesis of benzoic acid, Electrochimica Acta 470, 143377. https://doi.org/10.1016/j.electacta.2023.143377.

[11] Gao, D., Ouyang, D., Zhao, X. (2024). Controllable oxidative depolymerization of lignin to produce aromatic aldehydes and generate electricity under mild conditions with direct biomass fuel cells as flexible reactors, Chemical Engineering Journal 479, 147874. https://doi.org/10.1016/j.cej.2023.147874.

[12] Mohamad Ibrahim, M.N., Zakaria, N., Sipaut, C.S., Sulaiman, O., Hashim, R. (2011). Chemical and thermal properties of lignins from oil palm biomass as a substitute for phenol in a phenol formaldehyde resin production, Carbohydrate Polymers 86(1), 112-119. https://doi.org/10.1016/j.carbpol.2011.04.018.

[13] Wen, J.-L., Xue, B.-L., Xu, F., Sun, R.-C. (2012). Unveiling the structural heterogeneity of bamboo lignin by in situ HSQC NMR technique, BioEnergy Research 5(4), 886-903. https://doi.org/10.1007/s12155-012-9203-5.

[14] Abdelaziz, O.Y., Hulteberg, C.P. (2016). Physicochemical characterisation of technical lignins for their potential valorisation, Waste and Biomass Valorization 8(3), 859-869. https://doi.org/10.1007/s12649-016-9643-9.

[15] Esteves Costa, C.A., Coleman, W., Dube, M., Rodrigues, A.E., Rodrigues Pinto, P.C. (2016). Assessment of key features of lignin from lignocellulosic crops: Stalks and roots of corn, cotton, sugarcane, and tobacco, Industrial Crops and Products 92, 136-148. https://doi.org/10.1016/j.indcrop.2016.07.032.

[16] Fodil Cherif, M., Trache, D., Brosse, N., Benaliouche, F., Tarchoun, A.F. (2020). Comparison of the physicochemical properties and thermal stability of organosolv and Kraft lignins from hardwood and softwood biomass for their potential valorization, Waste and Biomass Valorization 11(12), 6541-6553. https://doi.org/10.1007/s12649-020-00955-0.

[17] Pinto, P.C.R., da Silva, E.A.B., Rodrigues, A.E. (2010). Comparative study of solid-phase extraction and liquid-liquid extraction for the reliable quantification of high value added compounds from oxidation processes of wood-derived lignin, Industrial & Engineering Chemistry Research 49(23), 12311-12318. https://doi.org/10.1021/ie101680s.

[18] International Organization for Standardization, ISO 3104:2020 - Petroleum products - Transparent and opaque liquids - Determination of kinematic viscosity and calculation of dynamic viscosity, 2020.